ACS APPLIED MATERIALS & INTERFACES

Research Article

Cite This: ACS Appl. Mater. Interfaces XXXX, XXX, XXX−XXX

www.acsami.org

Fully Water-Soluble, High-Performance Transient Sensors on a Versatile Galactomannan Substrate Derived from the Endosperm

Ning Yi,[†,▽] Zheng Cheng,[‡,▽] Lei Yang,[‡] Gregory Edelman,[§] Cuili Xue,[§,∥] Yi Ma,[‡] Hongli Zhu,[*,‡] and Huanyu Cheng[*,†,§]

[†]Department of Materials Science and Engineering and [§]Department of Engineering Science and Mechanics, Materials Research Institute, The Pennsylvania State University, University Park, Pennsylvania 16802, United States

[‡]Department of Mechanical and Industrial Engineering, Northeastern University, Boston, Massachusetts 02115, United States

[∥]School of Precision Instrument and Optoelectronics Engineering, Tianjin University, Tianjin 300072, China

Supporting Information

ABSTRACT: Green electronics on biodegradable substrates from natural sources have gained broad interest because of the advantages of being biodegradable, recyclable, sustainable, and cost-efficient. This study presents a low-cost, yet simple extraction and purification method that explores aqueous extraction and precipitation with ethanol for the synthesis of galactomannan films. In salient contrast to the other materials of natural origin, the process to obtain galactomannan films is energy efficient and environmentally friendly. As an alternative biodegradable material, galactomannan has direct relevance to the recent emerging biodegradable or transient electronics. The galactomannan substrate with temperature sensors and electrodes fabricated from zinc, a biodegradable material noted for its essential biological function, demonstrates a high-precision measurement of temperature and high-fidelity monitoring of electrophysiological signals (electromyogram or electrocardiogram). The resulting disposable sensors disappear without a trace in water and produce environmentally benign end products that could even be used for alkaline soil amendments. The set of materials explored in this study is also stable in organic solutions, enabling solvent-based fabrication that may be combined with recent advances in additive manufacturing techniques for a novel manufacturing method.

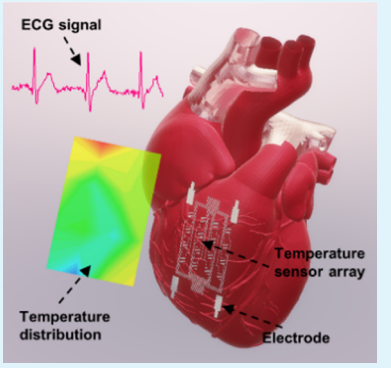

KEYWORDS: *galactomannan substrates, fully water soluble, green electronics, high-performance, biodegradable sensors*

INTRODUCTION

As rapid technological advances have led to a significant decrease in the lifetime of consumer electronics, an ever-growing number of electronic items are ending up in landfills (a total electronic waste of ∼3.2 M/year in the US[1,2]). To address such a long-standing challenge, it is of increasing interest to explore biodegradable materials for device fabrication, where the electronic systems disappear at controlled rates with environmentally benign end products when exposed to water. For instance, one can use an electronic component as a temporary monitor in the environment and allow it to safely dissolve on its own without the need for recollection.[3−5] This ability opens a wide range of applications from diagnostic/therapeutic implants[6−13] to permanent destruction of hardware for data security.[14,15]

Certain applications could, however, benefit from the utilization of natural renewable biomaterials as the substrate, in which the disposed devices could be recycled and further used in the environment (or even in the human body). Representative examples of materials with natural origin include gelatin,[16] shellac,[17] silk,[18] rice paper, and biodegradable cellulose nanofibril.[19] In comparison to the protein-based material such as gelatin and fibroin that consists repeating units of amino acids, galactomannan is a polysaccharide-based biomaterial associated with a simpler, greener, and more energy-efficient extraction process.[5,17] In addition, the galactomannan film exhibits a relatively good mechanical property and a certain degree of flexibility, whereas the gelatin and fibroin films are usually brittle because of the rigid partial double bond in the peptide chain resulted from the polar groups (i.e. C−N bond in the protein macromolecular).[20,21] Although biodegradable wood-derived polymers enable paper-based electronics, the large surface roughness of regular paper at the micrometer scale often triggers device failure.[22] As an alternative, a nanopaper made from nanocellulose (nanofiber or nanocrystal) has been explored for electronics fabrication.[22−28] However, the nanocellulose extraction process is typically associated with high energy and water consumption. The energy input to produce the cellulose nanofiber is between 20 000 and 30 000 kW h/t.[29] Meanwhile, the chemicals used to prepare nanocellulose, such as (2,2,6,6-tetramethylpiperidine-1-yl)oxidant for cellulose nanofiber preparation and 98%

Received: July 13, 2018
Accepted: September 28, 2018
Published: September 28, 2018

DOI: 10.1021/acsami.8b11682
ACS Appl. Mater. Interfaces XXXX, XXX, XXX−XXX

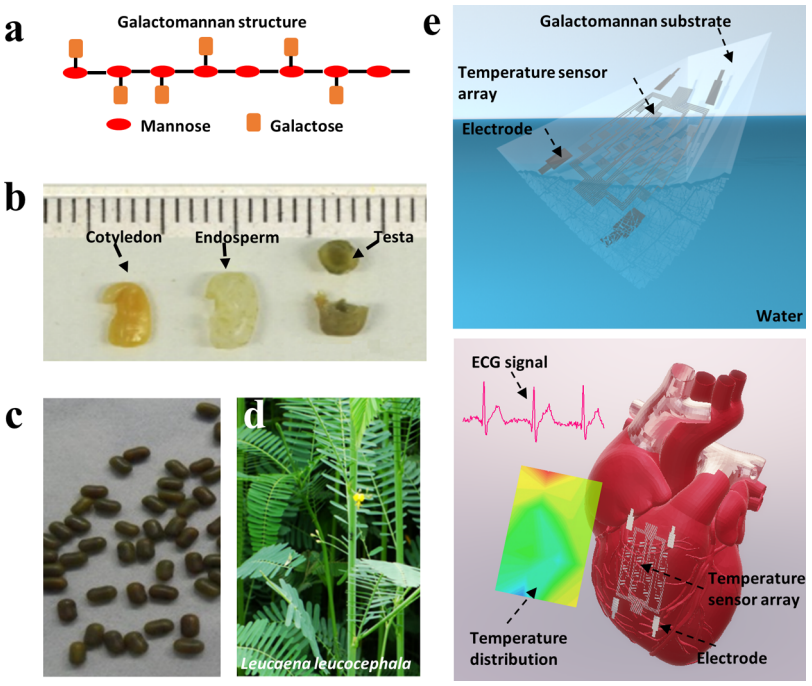

Figure 1. (a) Galactomannan consists of a mannose backbone and galactose side groups. (b) *Leucaena leucocephala* (*L. leucocephala*) is of comprised cotyledon, endosperm, and testa. (c) Digital image of the seeds of *L. leucocephala*. (d) Digital image of *L. leucocephala*. (e) Schematic illustration that shows the potential applications of the fully water-soluble, biodegradable sensors on an ultrathin galactomannan substrate partially dissolved in water upon immersion as disposable environmental sensors (top) or placed on a heart to potentially diagnose its arrhythmogenic disease states (bottom). The representative sensors could include arrays of temperature sensors for mapping temperature distribution and electrodes for electrophysiological signal measurements such as electrocardiogram (ECG).

H_2SO_4 for cellulose nanocrystal preparation, are toxic, corrosive, and costly. In addition, the cellulose nanopaper is not shape-stable in organic solvents, which is a big challenge for the device fabrication in organic solvents and indeed impedes its widescale industrial applications. The aforementioned challenges also hold true for other resorbable biomaterials that have been explored in the initial demonstration of transient electronics.

The central focus of transient electronics has been on the exploration of various materials toward a functional device. Similar to conventional circuits, critical components of transient electronics also include semiconductors, conductors, and insulators. Rapid developments of transient electronics have nucleated on a recent discovery[30] that single-crystal silicon can undergo hydrolysis to dissolve in biologically relevant conditions, that is, body temperature and near-neutral pH levels. Additional inorganic semiconducting materials explored for transient electronics also include ZnO[7] and Ge.[31] As for conductors, a variety of transient metals have been studied,[32] including Mg, Zn, Fe, Mo, and W. Biodegradable insulators that serve as passivation and encapsulation in microelectronics are also critical for the operation of the device.[11] In addition, they can serve as the substrate for the entire transient device to reside. Many early demonstrations[33,34] relied on synthetic biodegradable polymers or materials with a natural origin. Because of tunable properties, a wide range of synthetic biodegradable polymers[35−37] have been developed, including polyfluorene,[38] poly(vinyl alcohol),[33] polycaprolactone, and poly(lactic-*co*-glycolic acid), a copolymer of polylactic acid and polyglycolic acid.[39] However, to the best of our knowledge, no prior study has reported the use of galactomannan derived from the seeds of *Leucaena leucocephala* (*L. leucocephala*)as a water-soluble and biodegradable substrate for transient electric sensors.

Widely used in the food and biomedical industry, galactomannan, an earth-abundant reproducible polysaccharide, represents a promising alternative. The chemical structure (Figure 1a) of galactomannan consists of mannose backbone by β-1,4-glucosidic bonds and galactose side chains by α-1,6-glucosidic bonds, and the mannose/galactose (M/G) ratios differ depending on the botanic source.[40] Compared with other degradable materials, the galactomannan film has several unique features: (1) the extraction method is facile and scalable, where the galactomannan is extracted from the endosperm (Figure 1b) of the dicotyledonous seeds (Figure 1c) from *L. leucocephala* (Figure 1d),[41] *Cyamopsis tetragonoloba*,[42] and *Sesbania cannabina*[43] with low cost; (2) the aqueous extraction and ethanol purification method to obtain galactomannan is also more environmentally friendly and energy efficient when compared with that used for nanocellulose; (3) the water-soluble galactomannan substrate is shape-stable in an organic solvent, providing a good shape stability in an organic solvent based fabrication method. To demonstrate the application of galactomannan substrates toward transient electronics, a zinc thin film is patterned on the galactomannan film to form functional components in this study. Capable of temperature mapping and electrophysiological signal detection, the resulting device can enable potential diagnosing arrhythmogenic disease states of the heart (Figure 1e). As a proof-of-concept demonstration toward low-cost, fully biodegradable transient electronics, for the first time, we have fabricated a high-performance zinc-based 4 by 4 temperature sensor array and electrodes endowed on galactomannan substrates for continuous monitoring of

DOI: 10.1021/acsami.8b11682
ACS Appl. Mater. Interfaces XXXX, XXX, XXX−XXX

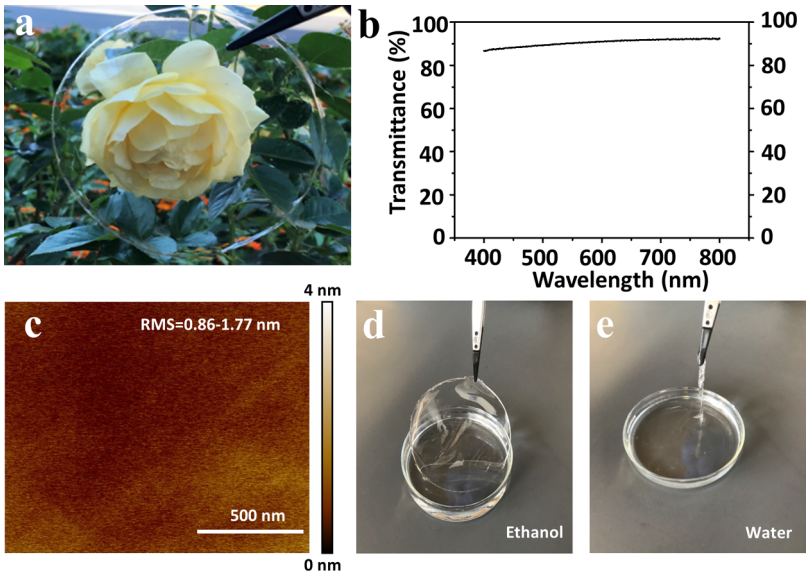

Figure 2. (a) Digital image of the galactomannan film with high optical transparency. (b) Light transmittance of the galactomannan film in the wavelength range of 400−800 nm. (c) Atomic force microscopy (AFM) image of the galactomannan film with a super smooth surface. (d) Galactomannan film maintained its shape after immersing in ethanol for 24 h. (e) Partially dissolved galactomannan film collapsed after immersing in water for 5 min.

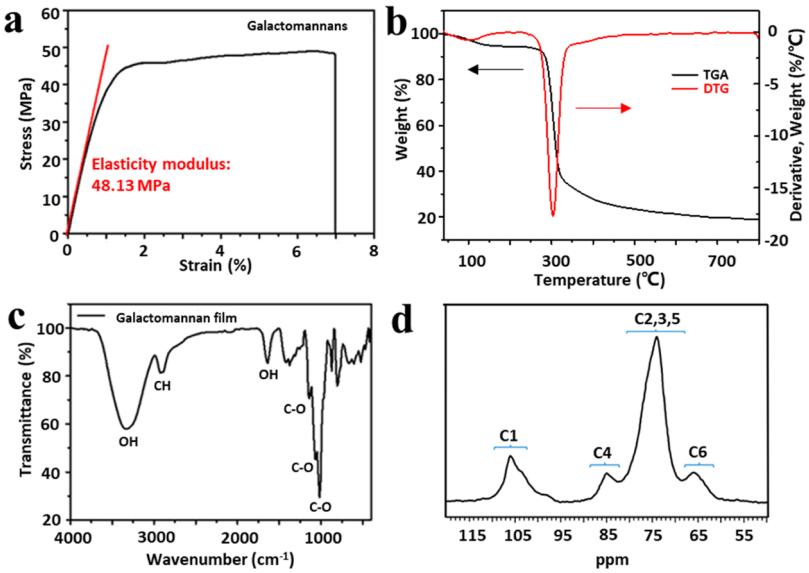

Figure 3. (a) Stress−strain curve of the galactomannan film measured from a uniaxial tensile test, with an elastic modulus of 48.13 MPa calculated from the linear range. (b) Thermogravimetric analysis (TGA) and derivative thermogravimetric (DTG, dW/dT) curves show the thermal stability of the galactomannan film. The maximum degradation rate occurs at 302 °C. (c) Fourier transfer infrared (FTIR) spectra curve of the galactomannan. (d) ^{13}C nuclear magnetic resonance (NMR) curve of galactomannan.

temperature variation and electrophysiological signals, respectively. This work paves the way to develop next-generation sustainable, biodegradable, and economical substrates, which are capable of superseding plastic to create greener electronics. Though the demonstrations as disposable environmental sensors or cardiac monitors are not carried out in this study, the literature and our previous studies on device integration[44−46] and cytotoxicity[47−49] have indicated the possibility toward the envisioned applications as in Figure 1e. Stable in the organic solvent, the biodegradable galactomannan also promises solvent-based fabrication processes that may be combined with recent advances in additive manufacturing techniques for a novel manufacturing method.

RESULTS AND DISCUSSION

The *L. leucocephala*'s seed endosperm was first grounded to 100 fine mesh powders. Next, the endosperm powder was dispersed in the water under mechanical stirring. After 24 h, the mixture was centrifuged at 10 000 rpm for 20 min, followed by a sufficient wash in ethanol. By using the freeze-dryer, the galactomannan powder with a purity of 99.0% was obtained in the resulting precipitate. The weight analysis of the seed structure indicates that the endosperm contains 58.65% of galactomannan in weight. The ratio of M/G is ca. 1.3:1, and the average molecular weight M_w is 1.26 × 10^6 Da. Dissolving 10 mg/mL of galactomannan in deionized water under mechanical stirring, the dispersion was then degassed for 20

DOI: 10.1021/acsami.8b11682
ACS Appl. Mater. Interfaces XXXX, XXX, XXX−XXX

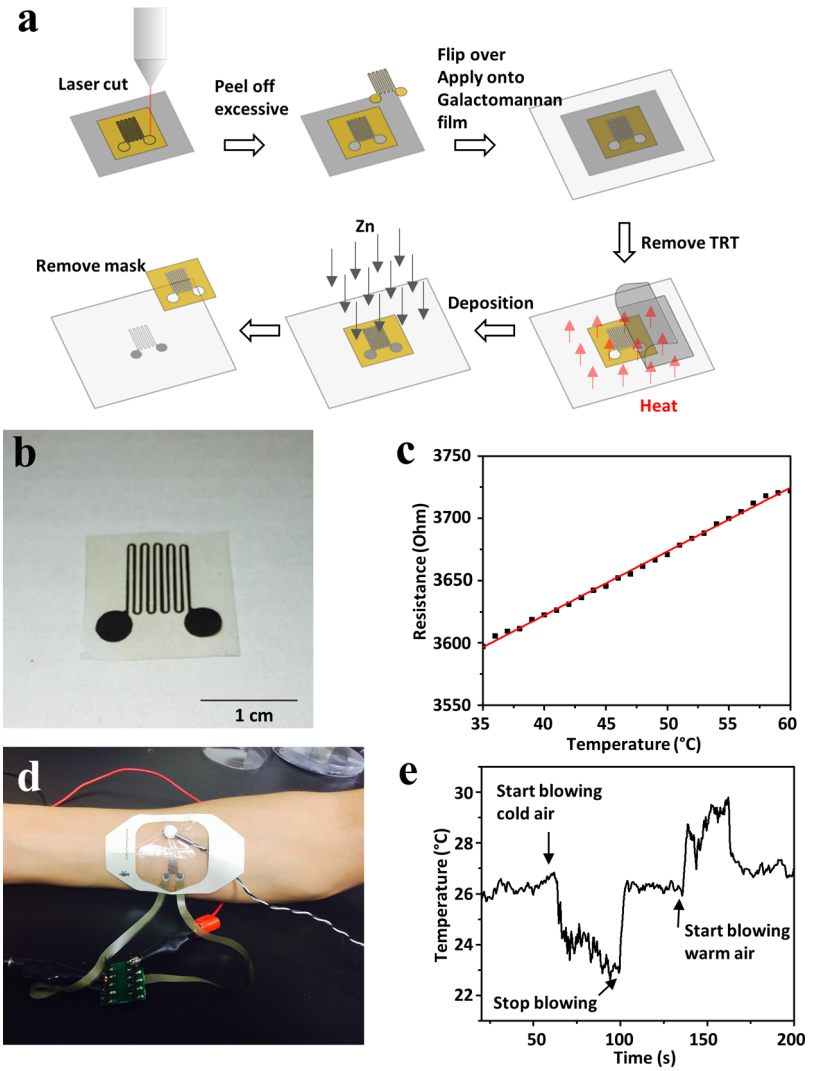

Figure 4. (a) Fabrication process of a zinc sensor through a laser-cut shadow mask. (b) Temperature sensor on the galactomannan substrate. (c) Calibration curve of the zinc temperature sensor where its resistance is shown as a function of temperature (symbol: experimental measurements; red line: fitted calibration curve). (d) On-skin temperature measurement setup. The commercial thermistor was fixed above the Zn sensor by the Tegaderm medical dressing. (e) Real-time temperature measurement from the Zn temperature sensor.

min in a bath sonicator until no bubbles were observed. Slowly pouring different volumes of the galactomannan suspension (10 mg/mL) into polystyrene petri dish and drying at an ambient temperature resulted in galactomannan films of various thicknesses. The aqueous extraction method can prepare galactomannan films with size in a wide range. Taken together with the fact that *L. leucocephala* is a fast-growing mimosoid tree with abundant volume in nature, the galactomannan films are suitable for potential large-scale production.

Galactomannan forms highly viscous colloidal aqueous solutions when hydrated in water, leading to easy fabrication of the film with an excellent optical transparency. The resulting galactomannan films are optically transparent (Figure 2a), and the transmittance property has been further investigated by UV−Vis spectrometer. The result, shown in Figure 2b, indicates that the film has a total optical transmittance of >85% in the wavelength range of 400−800 nm. The high transparency enables direct visualization of the tissues under the transparent film integrated with sensing devices. The excellent optical transmittance property could also find potential applications in optoelectronic devices, such as to increase the power output of light-emitting diodes. As revealed by a root mean square value between 0.86 and 1.77 nm from atomic force microscopy (AFM) (Figure 2c), the transparent substrate possesses a super smooth surface, beneficial for the device fabrication. When used as a dielectric material in transistors, the property may also provide enhanced device performance. Most importantly, the galactomannan films display a completely different stability in water and organic solvents (e.g., ethanol). Although the film is stable and maintains its structural integrity in ethanol after 24 h (Figure 2d), it completely disintegrates after immersing in water for only 5 min (Figure 2e).

The mechanical property of the galactomannan film plays an essential role in the integration of sensing devices. To quantify the mechanical property of the galactomannan film, the stress−strain curve of the film was measured in Figure 3a. From the stress−strain curve, the tensile strength and elastic modulus of the galactomannan film are obtained as 47.9 and 48.1 MPa, respectively. The thermal stability of the galactomannan film in the air was also studied. The corresponding thermogravimetric

DOI: 10.1021/acsami.8b11682
ACS Appl. Mater. Interfaces XXXX, XXX, XXX−XXX

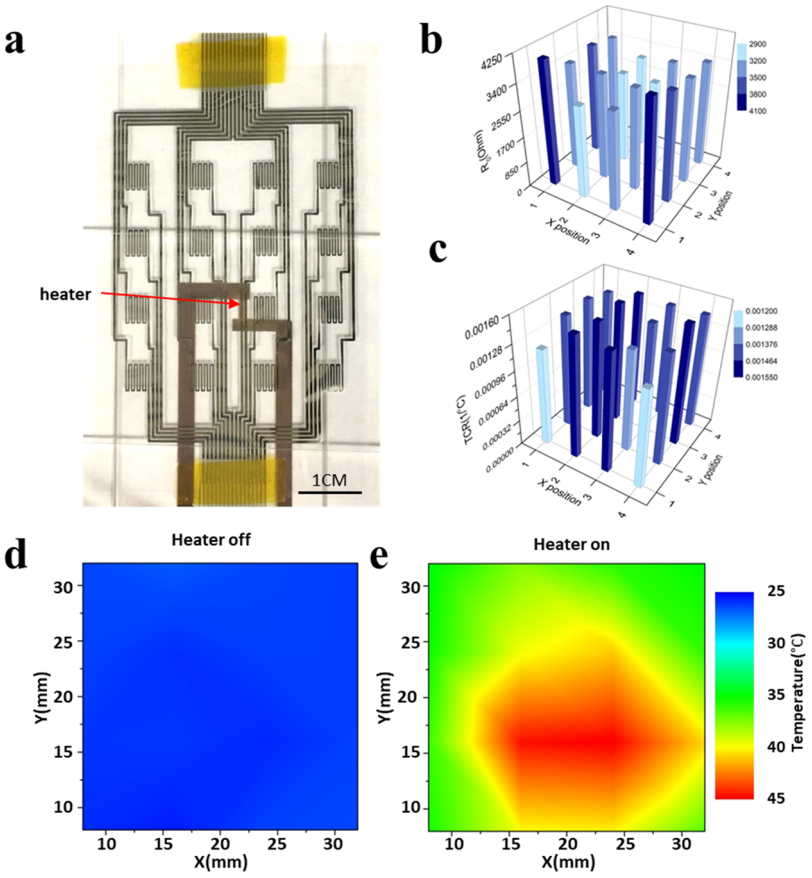

Figure 5. (a) Temperature sensor array on a heater, with the location indicated by the red arrow. (b) Reference resistance of 16 temperature sensors at the temperature of 0 °C. The position of the temperature sensor in (a) is indicated by numbers (*x*-axis: 1−4 indicates from left to right; *y*-axis: 1−4 indicates from bottom to top). (c) Temperature coefficient of resistance (TCR) of 16 temperature sensors obtained from the calibration curve. (d) Temperature mapping result before the heater was turned on. (e) Temperature mapping result after the heater was turned on for 5 min. The color map was depicted by OriginPro 8.5.

analysis (TGA) curve (Figure 3b) indicates that the initial weight loss appears from 80 to 150 °C because of the evaporation of free and bound water. The thermal decomposition of the galactomannan film happens from 300 to 400 °C, and the weight loss is approximately 80%. The thermal decomposition rate of the galactomannan film was calculated from the derivative TGA, indicating that the maximum degradation rate occurs at 302 °C (Figure 3b). This thermal analysis provides critical insight for device fabrication, as the modest temperature for the galactomannan film to be thermally stable requires a relatively low-temperature manufacturing of sensing devices.

The chemical groups of the galactomannan measured with FTIR spectra (Figure 3c) exhibit a principle absorption peak at 3400 cm^{-1} that corresponds to the stretching vibrations of the −OH group. This −OH group could enable us to program the properties of galactomannan further. The weak peak at 2900 cm^{-1} is attributed to the −CH stretching vibration. The representative spectrum shows a strong peak at 1600 cm^{-1}, corresponding to the −OH bending vibration. The representative peaks at 815 and 870 cm^{-1} are related with the anomeric glycosidic linkages, which are ascribed to α-D-galactopyranose and β-D-mannopyranose, respectively.[50,51] The strong absorption peaks of 1190 and 980 cm^{-1} corresponded to the stretching vibrations of C−O in the glycosidic bonds. In addition, the peak at 1150 cm^{-1} is assigned to the bending vibration of C−O groups.

Nuclear magnetic resonance (NMR) spectroscopy is an effective characterization tool indispensable for the analysis of chemical structure. Galactomannan extracted from the *L. leucocephala* seeds was analyzed by ^{13}C NMR spectroscopy. As a plant-derived heterogeneous polysaccharide, galactomannan consists of a mannose backbone with galactose side groups. As observed in Figure 3d, ^{13}C NMR analyses of polysaccharides have revealed specific carbohydrate signals that are characteristic of the galactomannan with low molecular weights. It can be seen that the ^{13}C NMR spectrum reveals well-resolved signals in the anomeric region, corresponding to the C1 of an α-D-galactopyranose at 106 ppm.[52] In addition, the signal at 85 ppm is associated with C4 of an unbranched β-D-mannopyranose at the O6 position.[53] Moreover, the 70−78 ppm region gives important information about the structure because of the specific strong signal at 73 ppm attributed to C2, C3, and C5 of β-D-mannopyranose branched at the O6 position. The signal at 66 ppm is assigned to C6 of the main chain mannopyranose with galactose branches.[54] Attempts have been made to draw the possible molecular structural formula based on the FTIR and NMR results that show the majority of functional groups. However, the other functional groups as well as the specific connection in between bonds (e.g., the C−C bond) are still needed before the molecular structural formula can be inferred.

Figure 4 demonstrates the deposition of biodegradable metals on a 50 μm thick galactomannan film to yield a passive temperature sensor. With increasing interest in applying tattoo-

DOI: 10.1021/acsami.8b11682
ACS Appl. Mater. Interfaces XXXX, XXX, XXX−XXX

like sensors in internet-of-things devices for human health, the potential exponential proliferation could lead to adverse environmental effects. In this context, the completely biodegradable sensors can uniquely address such a challenge by disintegrating in water with environmentally benign end products to eliminate waste streams. The temperature sensor for precision thermometry of the skin can provide clinically relevant information for many important aspects of the human physiology. The fabrication process started with cutting a single-sided adhesive Kapton film on thermal release tape (TRT) to form a shadow mask for water-dissolvable metal deposition (Figure 4a). The purpose of employing the TRT is to ensure a flat surface when applying the shadow mask to the galactomannan film. In this proof-of-concept demonstration, we focused on water-soluble, biodegradable metals such as zinc, which is important for its essential biological function and biodegradability.[32,55,56] Zn films deposited by magnetron sputtering (Kurt J Lesker CMS-18) formed patterned traces in the temperature sensor. The adhesive on the Kapton shadow mask helped ensure good contact between the shadow mask and the water-soluble substrate, leading to improved pattern precision in the temperature sensor. Removal of the Kapton shadow mask left the temperature sensor on the galactomannan substrate (Figure 4b).

The resulting temperature sensor was connected to a digital multimeter (DMM) (Hewlett-Packard, 34401A Multimeter) in a probe station (Cascade Microtech 11000) for calibration (Figure S1). Placing the temperature sensor on the stage of the probe station allowed accurate control of the temperature by the Cascade thermal system (Abbess's Snow River, −60 to 200 °C). During calibration, the temperature was ramped up from 35 to 60 °C with a step of 1 °C. At each step, the temperature was held constant for 25 s to ensure thermal equilibrium. A metal shield that enclosed the stage minimized the effect of airflow for enhanced accuracy. Resistances of the sensor at different temperatures were measured and recorded by the DMM. The resistance of a material scales linearly with the temperature by following the equation of $R = R_{ref}[1 + \alpha(T - T_{ref})]$, where R_{ref} is the measured resistance of the material at a reference temperature T_{ref}, and α is the temperature coefficient of resistance (TCR). Linear regression between resistance R and temperature T results in a TCR of 1.48×10^{-3} and a reference resistance of 3.42×10^{3} Ω at the reference temperature of 0 °C, with a coefficient of determination R^2 of 0.998 (Figure 4c). The TCR in the thin film Zn temperature sensor is ∼38.4% of that in bulk zinc (i.e. 3.85×10^{-3}).[57] The decrease of the TCR in the thin film can be explained by the Fuchs−Sondheimer model, which indicates that reduction of the bulk metal material in one dimension is associated with increased surface scattering that is temperature independent.[58] The increased contribution from surface scattering leads to increased resistance, thereby decreasing the TCR.

To demonstrate the high-fidelity temperature sensing, both the water-soluble, biodegradable Zn temperature sensor and a commercial thermistor were placed on the skin of the subject with a Tegaderm medical dressing (3M) for temperature measurement (Figure 4d). The subject was allowed to sit still during the temperature measurement. An air blower was then used to blow at room temperature (cold air) at the location of the sensors for 30 s. Then, the air blower was turned off for 30 s before blowing warm air at the sensor location for another 30 s. The real-time monitoring of the temperature from the biodegradable temperature sensor demonstrates the utility (Figure 4e). The sharp changes (i.e. a decrease induced from the cold air and increase an induced from the warm air) of the captured signal indicate the fast response of the water-soluble, biodegradable sensors for real-time body temperature sensing.

Integrating a single sensor in an array (Figure 5a) can also enable noninvasive spatial mapping of skin temperature, as well as simultaneous quantification of the thermal conductivity of the underlying tissues. As a first step toward this goal, a temperature sensor array of 4 by 4 was created by the electron beam (e-beam) evaporation (Semicore evaporator) of Zn through a patterned shadow mask (Figure S2a). The resulting temperature sensor array was flexible and capable of bending over a small radius (e.g., 1 cm) of curvature without damage (Figure S2b). Scanning electron microscopy (SEM) images (Nova NanoSEM630, FEI) were taken to show the pattern of one single temperature sensor. The surface of the deposited zinc by both e-beam evaporation and sputtering was also characterized by SEM (Figure S2c,d). When taken together with a multiplexing scheme, the temperature sensor array could be used for applications ranging from noninvasive spatial mapping to revelation of the time−dynamic influence of blood flow and perfusion, as demonstrated in our previous work on the ultrathin conformal temperature array.[59] To demonstrate the temperature mapping capability, a custom-built control circuit (Figure S3) was used to accomplish the multiplexing among temperature sensors in the array. The 4 by 4 temperature sensors were connected to the measuring unit (Keithley 2401 source meter) through anisotropic conductive films (ACFs), a SOIC-32 to DIP-32 SMT adapter board, a 16 channels relay (SainSmart), and an Arduino Mega 2560 microcontroller (Figure S3). The microcontroller enabled customizable multiplexing of the sensors and manual control of the relay, which facilitates the temperature mapping and the calibration of each sensor in the array. The reference resistance and the TCR of each temperature sensor were obtained through the same calibration procedure as aforementioned. The reference resistance from each temperature sensor at the reference temperature of 0 °C falls in the range from 3.01×10^{3} to 4.06×10^{3} Ω (Figure 5b), where the variation in resistance is attributed to the different lengths in the interconnect region of each sensor. The TCR of the temperature sensors ranges from 1.21×10^{-3} to 1.53×10^{-3} (Figure 5c). A simple patterned design of titanium with a thickness of 100 nm from e-beam evaporation on a glass slide yields a heater used in the demonstration of the temperature mapping. The heater can raise up the temperature by 21.6 °C (a digital thermometer, Digi-Sense) when a 1.5 V voltage is applied. The heating unit was placed below the transient temperature sensor array at the lower center of the array indicated by the red arrow in Figure 5a. Temperature mapping was performed before (Figure 5d) and 5 min after (Figure 5e) the heater was turned on, demonstrating the successful capture of the spatial mapping of the temperature.

Through the use of shadow mask deposition, patterned electrodes can also be obtained through either sputtering or e-beam evaporation. As a proof-of-concept demonstration, electrodes for the measurement of ECG and electromyogram (EMG) signals in a rectangular (10 mm by 2 mm) geometry were obtained through sputtering. In order to improve the contact quality and avoid the influence of the surface native oxide, small contact pads (4 mm by 8 mm) consisting a thin layer of chromium (5 nm) and gold (50 nm) were evaporated through Kapton shadow mask deposition on the galacto-

DOI: 10.1021/acsami.8b11682
ACS Appl. Mater. Interfaces XXXX, XXX, XXX−XXX

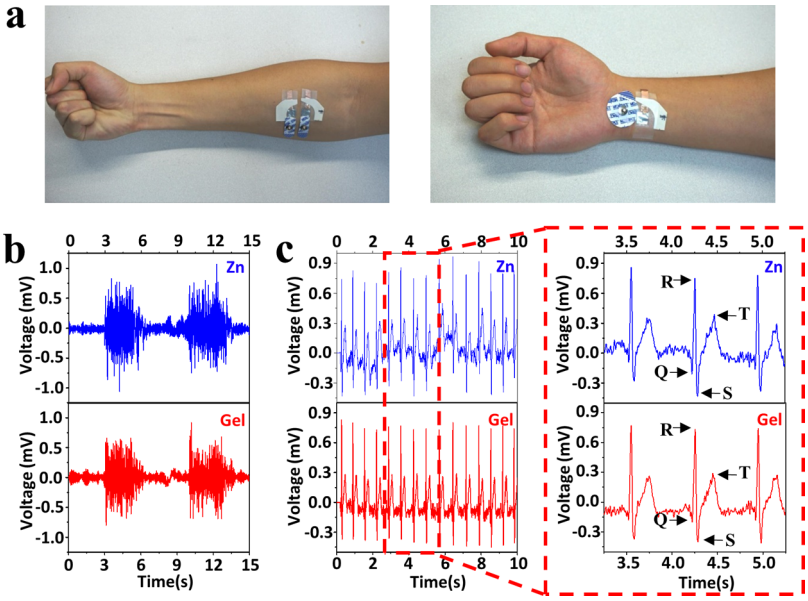

Figure 6. (a) Photographs showing the sensor locations for the measurement of electromyogram (EMG, left) and electrocardiogram (ECG, right) signals. (b) EMG signals collected from the Zn electrode and gel electrode. (c) ECG signals collected from the Zn electrode and the gel electrode. Baseline drift is observed in the ECG signal collected from the Zn electrode. A magnified view of the ECG signal in the inset shows PQRST waves.

mannan film prior to the deposition of the Zn electrode. A quarter of the Au contact pad overlapped with the sputtered Zn electrode (thickness of 100 nm) to provide electrical connection. Such a simple testing setup minimizes the effect of the Zn oxidation in an ambient environment on the contact impedance between the Zn electrode and flexible cables. The resulting electrodes were mechanically robust to deformations. To demonstrate such an idea, a rectangular (10 mm by 2 mm) Zn electrode with a thickness of 100 nm connected to two Au contact pads (50 nm) was fabricated on the galactomannan film through the Kapton shadow mask following the deposition method described earlier. The two contact pads of the electrode were clamped on a custom-built stainless steel stretcher. The connection between the electrode and a DMM was accomplished by silver epoxy paste (Silver Epoxy Adhesive 8331, MG Chemicals) and copper ribbons (Pyralux AC091200EV, DuPont). The resistance of the electrode only changed by less than 2% when a compressive strain up to 30% was applied to induce the bending of the electrode (Figure S4). The negligible change in the resistance is attributed to the small bending strain in the Zn electrode predicted by the theoretical analysis. Upon compression, the Zn electrode on the galactomannan substrate bends out-of-plane to take a sinusoidal shape $y = A \sin \frac{\pi x}{L_0(1-\varepsilon)}$, where y is the out-of-plane displacement of the film from its initial position, x is the coordinate along the initial film direction, A is the maximum displacement occurred at the midpoint of the film, L_0 = 12 mm is the initial distance between two clamps, and ε is the applied compressive strain. Upon a compressive strain of 30%, the maximum displacement A is determined to be 2.5 mm. The maximum bending strain in the Zn electrode is given as $\varepsilon_{peak} = y''|_{max} \cdot d$, where d is the distance from the top surface of the Zn layer to the neutral mechanical plane of the Zn-galactomannan double-layered composite.[60] The distance d is calculated from $d = \sum_{i=1}^{N} \overline{E}_i h_i \left(\sum_{j=1}^{i} h_j - \frac{1}{2} h_i \right) / \sum_{i=1}^{N} \overline{E}_i h_i$,[61] where N = 2 is the total number of layers in the composite, and $\overline{E_1} = \overline{E_{Zn}}$ = 115.2 GPa and $h_1 = h_{Zn}$ = 100 nm ($\overline{E_2} = \overline{E}_{galactomannan}$ = 64.17 MPa, $h_2 = h_{galactomannan}$ = 50 μm) are the plane strain Young's modulus and thickness of the zinc electrode (galactomannan film), respectively. The maximum bending strain in the Zn electrode is therefore calculated as 0.19%, which helps explain the small resistance variation.

Although simple in the device design, the electrodes are capable of monitoring electrophysiological processes related to the activity of the heart (electrocardiogram, ECG), muscle tissues (EMG), and the brain [electroencephalogram (EEG)]. The EEG signal monitoring can be quite challenging, partially because of poor signal-to-noise ratio (SNR) without proper signal amplification. Therefore, we focused on the monitoring of ECG and EMG signals in this study. PowerLab (16/35, ADInstruments) with BioAmp modules (Octal BioAmp, ADInstruments) served as the hardware for data acquisition and analysis for both ECG and EMG signals. A copper/polyimide laminate film (Pyralux AC091200EV, DuPont) was cut into thin ribbons to connect the sensor with the data acquisition system. One end of the copper ribbons was bonded to the gold contact pad via a small amount of silver epoxy paste, and the other end was connected to the BioAmp through microhooks. Commercially available silver/silver chloride (Ag/AgCl) gel electrodes were also placed in the vicinity of disposable sensors on the skin for direct comparison. Slightly different from the measurement setup that uses commercial Ag/AgCl gel electrodes, the Zn electrodes were placed on the surface of the forearm with a Tegaderm medical dressing to ensure good adhesion and comfort.

EMG signals were collected with the Zn electrodes placed along the direction of the flexor muscle (Figure 6a, left). Measurements were recorded with the subject clinching the hand every 7 s. Passing the output of the electrode to a digital 500 Hz low-pass filter followed by an analog-to-digital converter in the PowerLab system yielded data at a sampling rate of 1 kHz. A 60 Hz analog notch filter was applied in the BioAmp to filter out the power line noise. A 500 Hz low-pass filter was also chosen to filter out high-frequency noise in the

DOI: 10.1021/acsami.8b11682
ACS Appl. Mater. Interfaces XXXX, XXX, XXX−XXX

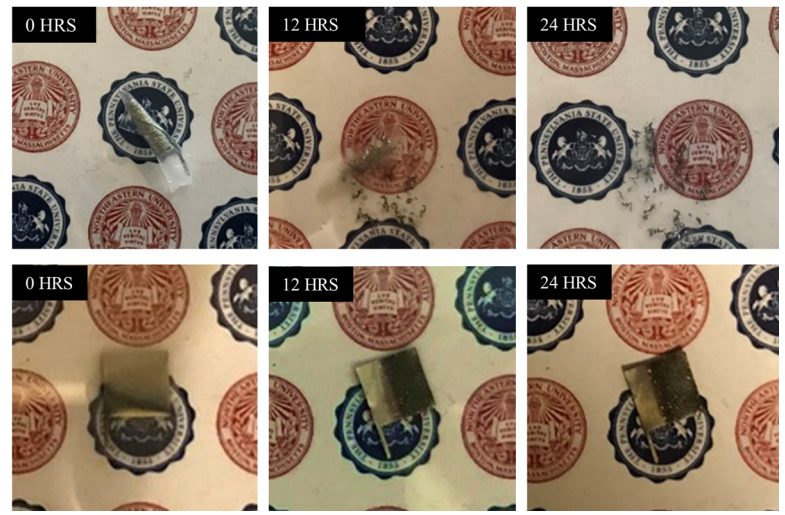

Figure 7. (a) Sequence of images shows the dissolution of the Zn electrode in water, where sensor rolled up at the beginning of the dissolution process. (b) Sequence of images shows that the Zn electrode is stable in ethanol. Photo credit: H. Cheng, Penn State University and Northeastern University.

EMG signal. The EMG signal collected from the Zn electrodes was compared with those from the commercial gel electrodes of the similar size (Figure 6b). The excellent level of agreement in EMG signals captured by the biodegradable zinc electrodes and Ag/AgCl gel electrodes establishes the precision of EMG signal measurement. The SNR of captured EMG signal was calculated by the SNR function in MATLAB using 2 s of signal and 2 s of the noise. The SNR value of the signal collected from the Zn electrodes is only slightly larger than that of the commercial gel electrodes, indicating a high-fidelity sensing capability from the Zn electrodes. The measurement repeated 15 days later still showed a relatively high SNR. A slight decrease in SNR from 15.57 ± 0.76 to 11.28 ± 0.49 for EMG and from 25.76 ± 1.15 to 23.06 ± 1.75 for ECG indicates the minimum effect of the surface oxidation on the measurement (Figure S5). The contact impedance between the electrode and the skin surface was also measured by an LCR meter, after 15 days of the sensor fabrication (Figure S6).

A three-lead setup enabled real-time recording of ECG using the Zn electrode on the water-soluble substrate. The measurement and reference electrodes were placed on the left and right front wrists (Figure 6a, right), and the ground electrode was placed on the left ankle. A digital 55 Hz low-pass filter was applied to eliminate high-frequency noise. Figure 6c presents a direct comparison between the ECG signals collected from the Zn electrodes and commercial gel electrodes. The SNR value of the ECG signal was also calculated following the definition of SNR = 20 $\log(V_s/V_n)$, where V_s is the peak-to-peak value (between the R peak and S peak) of the signal and V_n is the peak-to-peak value of the noise.[62] In such a definition, the signal refers to the PQRST waves, and the noise refers to all the other portions of the data that are not PQRST waves. Because of the high SNR value in the ECG signals collected from the Zn electrodes (slightly higher than that from the commercial gel electrode), characteristic features such as PQRST waves can be identified. The EMG and ECG signals collected from nonbiodegradable Cu electrodes are also compared to those from commercial gel electrodes (Figure S7a,b). Given the comparison to the common commercial gel electrode, the biodegradable Zn electrodes have demonstrated performance comparable to the nonbiodegradable electrodes. It should be noted that the baseline drift of ECG signals collected from both Cu and Zn electrodes is likely attributed to respiration or body movement.[63]

Dissolution behavior of the disposable sensors (e.g., electrodes or temperature sensors) was studied by placing them in ethanol and distilled water for 24 h, respectively. It can be observed that the disposable sensors disintegrated and most of the device components were dissolved in water (Figure 7a) but remained stable in ethanol (Figure 7b). Because of the patterned geometry, the temperature sensor dissolved slightly quicker than that of the electrode (Figure S8). It should also be noted that the dissolution of the Zn electrode leads to visible bubbles of hydrogen trapped between the Zn electrode and the Petri dish when the Zn electrode was taped (Figure S9).

CONCLUSIONS

In summary, we rationally designed a simple extraction and purification method to obtain low-cost, energy-efficient, environmentally friendly, fully water-soluble galactomannan films. Building on the galactomannan substrate, we demonstrated for the first time that high-performance zinc-based sensors could be used for high-precision temperature mapping and high-fidelity electrophysiological signal monitoring. When combined with the device integration[44−46] and cytotoxicity[47−49] studies of this set of materials, the proof-of-concept demonstration presented in this study could easily be applied as disposable environmental sensors or biomedical devices. The resulting fully water-soluble sensors that disappear without a trace in water produce environmentally benign end products, which can even be used for alkaline soil amendments.[64] This work paves the way for the development of sustainable, economical, and disposable devices comprising biodegradable and earth-abundant materials to promote greener electronics. The materials explored for water-soluble sensors in this study are stable in organic solutions, which could further be explored in solvent-based fabrication. When taken together with novel additive manufacturing capabilities, this set of materials could open up a new manufacturing method of biodegradable electronics for a broad range of practical applications from biomedicine to green electronics for the environment.

DOI: 10.1021/acsami.8b11682
ACS Appl. Mater. Interfaces XXXX, XXX, XXX−XXX

EXPERIMENTAL SECTION

Materials. *L. leucocephala* seeds were obtained from Hebei Baiwei Biotechnology Co. LTD. Ethanol (99.5 wt %) was purchased from Fisher Scientific. All other chemicals were of analytical reagent grade and were used directly without further purification.

AFM Test. The galactomannan film was characterized using the fast scan dimension atomic force microscope (Bruker, USA). A mica substrate was used for the sample preparation, and AFM was performed in the tapping mode of operation with a scan rate of 1.85 Hz using silicon cantilevers (force constant 18 N/m, resonance frequency 1400 kHz).

Mechanical Test. The mechanical properties of the film were investigated using an electronic universal testing machine (Shimadzu, AG-Xplus). The 60 μm thickness of the galactomannan film was cut to a 0.5 × 6 cm rectangle, and the stretch rate was set at 1.0 mm/min. The Young's modulus was calculated according to the stress versus strain curve in the linear range.

UV−Vis Spectrum. Light transmittance spectra of the galactomannan films were measured from 400 to 800 nm with a TFProbe spectroscopic reflectometer (Agilent 8453, USA).

FTIR Test. The galactomannan powder was completely mixed with KBr and crushed into a superfine powder using a mortar and a pestle. The mixture was then pressed into a KBr pellet and then moved into a desiccator for 24 h at a temperature of 100 °C. The FTIR spectra recorded ranged from 4000 to 400 cm^{-1} on an FTIR instrument (Nicolet, USA).

TGA Test. The degradation property of galactomannan film was measured by the Netzsch STA 409 PC (TGA instrument, Germany). The sample was heated in air at a rate of 10 °C/min. The test temperature was set at a range of 40−800 °C.

NMR Test. The ^{13}C NMR spectra were recorded from 10 mg of purified galactomannan in 1 mL of D_2O on a Bruker AVANCE 600 MHz spectrometer equipped with a 5 mm broadband observe probe using an inverse-gated proton-decoupling sequence. Then, the solution was transferred to the Shigemi microtube and characterized at 25 °C. The detailed acquisition parameters were a 90 pulse width, a relaxation delay of 1.7 s, and an acquisition time of 1.2 s. A total of 20 000 scans were collected. The 2D data set was processed with 1000 and 91 000 data points using a Qsine function in both dimensions.

Fabrication Process of Biodegradable Electronics on Galactomannan Films. Cutting a piece of Kapton tape (polyimide film tape 5413 Amber, 3M) with single-sided adhesive and a thickness of 75 μm by a CO_2 laser (Universal Laser System, M360) formed a shadow mask for Zn deposition. The Kapton film on a TRT (Semiconductor Corp) was fixed on top of an alumina plate by using a Magic tape (3M). Attention was given to minimize air bubbles while laminating the Kapton film on the TRT for enhanced laser cutting quality. The laser cutting conditions were 7% power and 5% speed to achieve a high-quality shadow mask. Careful removal of the excessive region in the Kapton film by tweezers was followed by cleaning the Kapton shadow mask on the TRT in an ultrasonic water bath (Branson Ultrasonic, Branson 200) for 1 min. After water evaporation, leaving the sample on a hot plate (Scilogex, MS-H280-pro) at 90 °C released the Kapton shadow mask on the galactomannan films. Zn films deposited by magnetron sputtering (Kurt J Lesker CMS-18) formed patterned traces. The deposition conditions were 200 W, 5 μT for 2000 s. These conditions minimize delamination and maintain high quality, uniform films with good yield. The adhesive on the Kapton shadow mask also helped ensure good contact between the shadow mask and the water-soluble substrate. Removal of the Kapton shadow mask left the sensor on the water-soluble substrate.

Experiments on Human Subjects. All experiments on human skin were conducted under the approval from the Institutional Review Board of The Pennsylvania State University (protocol number STUDY00008003), and volunteer subjects gave informed consent.

Temperature Mapping Experiment. The temperature sensor array was connected to the SOIC-32 to DIP-32 SMT adaptor board by heat pressing (330 °F) the ACF tape for 5 s onto the galactomannan film and board separately. L-shape 2.54 mm pitch pin headers were soldered onto the SMT pad to ensure a good connection between the adaptor board and relay board through DuPont male-to-female breadboard jumper wires (DuPont). The 16 channel relay had its switches connected to the SOIC-32 to DIP-32 SMT adaptor and its control panel pins connected to the Arduino Mega 2560 microcontroller. The USB interface of Arduino Mega 2560 enabled the customized coding of the microcontroller by desktop using the Arduino IDE programming software. A multiplexing rate of 2 Hz was employed for the temperature mapping.

ASSOCIATED CONTENT

Supporting Information

The Supporting Information is available free of charge on the ACS Publications website at DOI: 10.1021/acsami.8b11682.

Experimental setup for the calibration of the temperature sensor, optical and SEM images of a temperature sensor array, schematic diagram of the multiplexing circuit for the temperature sensor array, resistance measurement of water-soluble electrodes upon bending, contact impedance of water-soluble electrodes, EMG and ECG signals collected from water-soluble electrodes and copper electrodes, and dissolution test of the temperature sensor and electrodes (PDF)

AUTHOR INFORMATION

Corresponding Authors

*E-mail: h.zhu@neu.edu (H.Z.).
*Email: huanyu.cheng@psu.edu (H.C.).

ORCID

Lei Yang: 0000-0001-9600-7589
Hongli Zhu: 0000-0003-1733-4333
Huanyu Cheng: 0000-0001-6075-4208

Author Contributions

▽N.Y. and Z.C. contributed equally. The manuscript was written through contributions from all authors. All authors have given approval to the final version of the manuscript.

Funding

This work is supported by the start-up grant and Tier 1 fund to H.Z. from the Northeastern University and the start-up fund provided to H.C. by the Engineering Science and Mechanics Department, College of Engineering, and Materials Research Institute at The Pennsylvania State University. H.C. also acknowledges the support from ASME Haythornthwaite Foundation Research Initiation Grant and Dorothy Quiggle Career Development Professorship in Engineering and Global Engineering Leadership Program at Penn State.

Notes

The authors declare no competing financial interest.

ACKNOWLEDGMENTS

N.Y. and H.C. would like to thank Jia Zhu, Tianqi Wang, and Yudi Wang for their help with the human subject research. The help from Mark Pauley on SEM imaging and from Prof. Andy Zhou at the Indiana University of Pennsylvania on the e-beam evaporation of Zn is also acknowledged.

REFERENCES

(1) Lorenzen, J. A. Green Consumption and Social Change: Debates over Responsibility, Private Action, and Access. *Sociol. Compass* **2014**, *8*, 1063−1081.

DOI: 10.1021/acsami.8b11682
ACS Appl. Mater. Interfaces XXXX, XXX, XXX−XXX

(2) Pramila, S.; Fulekar, M.; Bhawana, P. E-Waste-a Challenge for Tomorrow. *Res. J. Recent Sci.* **2012**, *1*, 86−93.
(3) Jung, Y. H.; Chang, T.-H.; Zhang, H.; Yao, C.; Zheng, Q.; Yang, V. W.; Mi, H.; Kim, M.; Cho, S. J.; Park, D.-W. High-Performance Green Flexible Electronics Based on Biodegradable Cellulose Nanofibril Paper. *Nat. Commun.* **2015**, *6*, 7170.
(4) Hwang, S.-W.; Song, J.-K.; Huang, X.; Cheng, H.; Kang, S.-K.; Kim, B. H.; Kim, J.-H.; Yu, S.; Huang, Y.; Rogers, J. A. High-Performance Biodegradable/Transient Electronics on Biodegradable Polymers. *Adv. Mater.* **2014**, *26*, 3905−3911.
(5) Irimia-Vladu, M.; Głowacki, E. D.; Voss, G.; Bauer, S.; Sariciftci, N. S. Green and Biodegradable Electronics. *Mater. Today* **2012**, *15*, 340−346.
(6) Hwang, S.-W.; Tao, H.; Kim, D.-H.; Cheng, H.; Song, J.-K.; Rill, E.; Brenckle, M. A.; Panilaitis, B.; Won, S. M.; Kim, Y.-S.; Song, Y. M.; Yu, K. J.; Ameen, A.; Li, R.; Su, Y.; Yang, M.; Kaplan, D. L.; Zakin, M. R.; Slepian, M. J.; Huang, Y.; Omenetto, F. G.; Rogers, J. A. A Physically Transient Form of Silicon Electronics. *Science* **2012**, *337*, 1640−1644.
(7) Dagdeviren, C.; Hwang, S.-W.; Su, Y.; Kim, S.; Cheng, H.; Gur, O.; Haney, R.; Omenetto, F. G.; Huang, Y.; Rogers, J. A. Transient, Biocompatible Electronics and Energy Harvesters Based on Zno. *Small* **2013**, *9*, 3398−3404.
(8) Hwang, S.-W.; Park, G.; Cheng, H.; Song, J.-K.; Kang, S.-K.; Yin, L.; Kim, J.-H.; Omenetto, F. G.; Huang, Y.; Lee, K.-M.; Rogers, J. A. 25th Anniversary Article: Materials for High-Performance Biodegradable Semiconductor Devices. *Adv. Mater.* **2014**, *26*, 1992−2000.
(9) Yin, L.; Cheng, H.; Mao, S.; Haasch, R.; Liu, Y.; Xie, X.; Hwang, S.-W.; Jain, H.; Kang, S.-K.; Su, Y.; Li, R.; Huang, Y.; Rogers, J. A. Dissolvable Metals for Transient Electronics. *Adv. Funct. Mater.* **2014**, *24*, 645−658.
(10) Hwang, S.-W.; Park, G.; Edwards, C.; Corbin, E. A.; Kang, S.-K.; Cheng, H.; Song, J.-K.; Kim, J.-H.; Yu, S.; Ng, J.; Lee, J. E.; Kim, J.; Yee, C.; Bhaduri, B.; Su, Y.; Omennetto, F. G.; Huang, Y.; Bashir, R.; Goddard, L.; Popescu, G.; Lee, K.-M.; Rogers, J. A. Dissolution Chemistry and Biocompatibility of Single-Crystalline Silicon Nanomembranes and Associated Materials for Transient Electronics. *ACS Nano* **2014**, *8*, 5843−5851.
(11) Kang, S.-K.; Hwang, S.-W.; Cheng, H.; Yu, S.; Kim, B. H.; Kim, J.-H.; Huang, Y.; Rogers, J. A. Dissolution Behaviors and Applications of Silicon Oxides and Nitrides in Transient Electronics. *Adv. Funct. Mater.* **2014**, *24*, 4427−4434.
(12) Kang, S.-K.; Park, G.; Kim, K.; Hwang, S.-W.; Cheng, H.; Shin, J.; Chung, S.; Kim, M.; Yin, L.; Lee, J. C.; Lee, K.-M.; Rogers, J. A. Dissolution Chemistry and Biocompatibility of Silicon- and Germanium-Based Semiconductors for Transient Electronics. *ACS Appl. Mater. Interfaces* **2015**, *7*, 9297−9305.
(13) Darouiche, R. O. Treatment of Infections Associated with Surgical Implants. *N. Engl. J. Med.* **2004**, *350*, 1422−1429.
(14) Lee, C. H.; Kang, S.-K.; Salvatore, G. A.; Ma, Y.; Kim, B. H.; Jiang, Y.; Kim, J. S.; Yan, L.; Wie, D. S.; Banks, A.; Oh, S. J.; Feng, X.; Huang, Y.; Troester, G.; Rogers, J. A. Wireless Microfluidic Systems for Programmed, Functional Transformation of Transient Electronic Devices. *Adv. Funct. Mater.* **2015**, *25*, 5100−5106.
(15) Lee, C. H.; Jeong, J.-W.; Liu, Y.; Zhang, Y.; Shi, Y.; Kang, S.-K.; Kim, J.; Kim, J. S.; Lee, N. Y.; Kim, B. H.; Jang, K.-I.; Yin, L.; Kim, M. K.; Banks, A.; Paik, U.; Huang, Y.; Rogers, J. A. Materials and Wireless Microfluidic Systems for Electronics Capable of Chemical Dissolution on Demand. *Adv. Funct. Mater.* **2015**, *25*, 1338−1343.
(16) Kim, Y. J.; Chun, S.-E.; Whitacre, J.; Bettinger, C. J. Self-Deployable Current Sources Fabricated from Edible Materials. *J. Mater. Chem. B* **2013**, *1*, 3781−3788.
(17) Irimia-Vladu, M. "Green" electronics: biodegradable and biocompatible materials and devices for sustainable future. *Chem. Soc. Rev.* **2014**, *43*, 588−610.
(18) Kim, D.-H.; Kim, Y.-S.; Amsden, J.; Panilaitis, B.; Kaplan, D. L.; Omenetto, F. G.; Zakin, M. R.; Rogers, J. A. Silicon Electronics on Silk as a Path to Bioresorbable, Implantable Devices. *Appl. Phys. Lett.* **2009**, *95*, 133701.
(19) Jung, Y. H.; Chang, T.-H.; Zhang, H.; Yao, C.; Zheng, Q.; Yang, V. W.; Mi, H.; Kim, M.; Cho, S. J.; Park, D.-W.; Jiang, H.; Lee, J.; Qiu, Y.; Zhou, W.; Cai, Z.; Gong, S.; Ma, Z. High-Performance Green Flexible Electronics Based on Biodegradable Cellulose Nanofibril Paper. *Nat. Commun.* **2015**, *6*, 7170.
(20) Peña, C.; de la Caba, K.; Eceiza, A.; Ruseckaite, R.; Mondragon, I. Enhancing Water Repellence and Mechanical Properties of Gelatin Films by Tannin Addition. *Bioresour. Technol.* **2010**, *101*, 6836−6842.
(21) Yin, J.; Chen, E.; Porter, D.; Shao, Z. Enhancing the Toughness of Regenerated Silk Fibroin Film through Uniaxial Extension. *Biomacromolecules* **2010**, *11*, 2890−2895.
(22) Huang, J.; Zhu, H.; Chen, Y.; Preston, C.; Rohrbach, K.; Cumings, J.; Hu, L. Highly Transparent and Flexible Nanopaper Transistors. *ACS Nano* **2013**, *7*, 2106−2113.
(23) Bao, W.; Fang, Z.; Wan, J.; Dai, J.; Zhu, H.; Han, X.; Yang, X.; Preston, C.; Hu, L. Aqueous Gating of Van Der Waals Materials on Bilayer Nanopaper. *ACS Nano* **2014**, *8*, 10606−10612.
(24) Fang, Z.; Zhu, H.; Preston, C.; Han, X.; Li, Y.; Lee, S.; Chai, X.; Chen, G.; Hu, L. Highly Transparent and Writable Wood All-Cellulose Hybrid Nanostructured Paper. *J. Mater. Chem. C* **2013**, *1*, 6191−6197.
(25) Hu, L.; Zheng, G.; Yao, J.; Liu, N.; Weil, B.; Eskilsson, M.; Karabulut, E.; Ruan, Z.; Fan, S.; Bloking, J. T.; McGehee, M. D.; Wågberg, L.; Cui, Y. Transparent and Conductive Paper from Nanocellulose Fibers. *Energy Environ. Sci.* **2013**, *6*, 513−518.
(26) Nogi, M.; Komoda, N.; Otsuka, K.; Suganuma, K. Foldable Nanopaper Antennas for Origami Electronics. *Nanoscale* **2013**, *5*, 4395−4399.
(27) Svagan, A. J.; Busko, D.; Avlasevich, Y.; Glasser, G.; Baluschev, S.; Landfester, K. Photon Energy Upconverting Nanopaper: A Bioinspired Oxygen Protection Strategy. *ACS Nano* **2014**, *8*, 8198−8207.
(28) Zhu, H.; Xiao, Z.; Liu, D.; Li, Y.; Weadock, N. J.; Huang, J.; Hu, L.; Fang, Z. Biodegradable Transparent Substrates for Flexible Organic-Light-Emitting Diodes. *Energy Environ. Sci.* **2013**, *6*, 2105.
(29) Siró, I.; Plackett, D. Microfibrillated Cellulose and New Nanocomposite Materials: A Review. *Cellulose* **2010**, *17*, 459−494.
(30) Hwang, S.-W.; Tao, H.; Kim, D.-H.; Cheng, H.; Song, J.-K.; Rill, E.; Brenckle, M. A.; Panilaitis, B.; Won, S. M.; Kim, Y.-S.; Song, Y. M.; Yu, K. J.; Ameen, A.; Li, R.; Su, Y.; Yang, M.; Kaplan, D. L.; Zakin, M. R.; Slepian, M. J.; Huang, Y.; Omenetto, F. G.; Rogers, J. A. A Physically Transient Form of Silicon Electronics. *Science* **2012**, *337*, 1640−1644.
(31) Kang, S.-K.; Park, G.; Kim, K.; Hwang, S.-W.; Cheng, H.; Shin, J.; Chung, S.; Kim, M.; Yin, L.; Lee, J. C.; Lee, K.-M.; Rogers, J. A. Dissolution Chemistry and Biocompatibility of Silicon- and Germanium-Based Semiconductors for Transient Electronics. *ACS Appl. Mater. Interfaces* **2015**, *7*, 9297−9305.
(32) Yin, L.; Cheng, H.; Mao, S.; Haasch, R.; Liu, Y.; Xie, X.; Hwang, S.-W.; Jain, H.; Kang, S.-K.; Su, Y.; Li, R.; Huang, Y.; Rogers, J. A. Dissolvable Metals for Transient Electronics. *Adv. Funct. Mater.* **2014**, *24*, 645−658.
(33) Bettinger, C. J.; Bao, Z. Organic Thin-Film Transistors Fabricated on Resorbable Biomaterial Substrates. *Adv. Mater.* **2010**, *22*, 651−655.
(34) Hwang, S.-W.; Lee, C. H.; Cheng, H.; Jeong, J.-W.; Kang, S.-K.; Kim, J.-H.; Shin, J.; Yang, J.; Liu, Z.; Ameer, G. A.; Huang, Y.; Rogers, J. A. Biodegradable Elastomers and Silicon Nanomembranes/Nanoribbons for Stretchable, Transient Electronics, and Biosensors. *Nano Lett.* **2015**, *15*, 2801−2808.
(35) Middleton, J. C.; Tipton, A. J. Synthetic Biodegradable Polymers as Orthopedic Devices. *Biomaterials* **2000**, *21*, 2335−2346.
(36) Tian, H.; Tang, Z.; Zhuang, X.; Chen, X.; Jing, X. Biodegradable Synthetic Polymers: Preparation, Functionalization and Biomedical Application. *Prog. Polym. Sci.* **2012**, *37*, 237−280.
(37) Nair, L. S.; Laurencin, C. T. Biodegradable Polymers as Biomaterials. *Prog. Polym. Sci.* **2007**, *32*, 762−798.
(38) Khanra, S.; Cipriano, T.; Lam, T.; White, T. A.; Fileti, E. E.; Alves, W. A.; Guha, S. Self-Assembled Peptide-Polyfluorene Nano-

DOI: 10.1021/acsami.8b11682
ACS Appl. Mater. Interfaces XXXX, XXX, XXX−XXX

composites for Biodegradable Organic Electronics. *Adv. Mater. Interfaces* **2015**, *2*, 1500265.
(39) Hwang, S.-W.; Song, J.-K.; Huang, X.; Cheng, H.; Kang, S.-K.; Kim, B. H.; Kim, J.-H.; Yu, S.; Huang, Y.; Rogers, J. A. High-Performance Biodegradable/Transient Electronics on Biodegradable Polymers. *Adv. Mater.* **2014**, *26*, 3905−3911.
(40) Kök, M. S.; Hill, S. E.; Mitchell, J. R. Viscosity of Galactomannans During High Temperature Processing: Influence of Degradation and Solubilisation. *Food Hydrocolloids* **1999**, *13*, 535−542.
(41) Mittal, N.; Mattu, P.; Kaur, G. Extraction and Derivatization of Leucaena Leucocephala (Lam.) Galactomannan: Optimization and Characterization. *Int. J. Biol. Macromol.* **2016**, *92*, 831−841.
(42) Gresta, F.; Sortino, O.; Santonoceto, C.; Issi, L.; Formantici, C.; Galante, Y. M. Effects of Sowing Times on Seed Yield, Protein and Galactomannans Content of Four Varieties of Guar (Cyamopsis Tetragonoloba L.) in a Mediterranean Environment. *Ind. Crops Prod.* **2013**, *41*, 46−52.
(43) Siddhuraju, P.; Osoniyi, O.; Makkar, H. P. S.; Becker, K. Effect of Soaking and Ionising Radiation on Various Antinutritional Factors of Seeds from Different Species of an Unconventional Legume, Sesbania and a Common Legume, Green Gram (Vigna Radiata). *Food Chem.* **2002**, *79*, 273−281.
(44) Xu, L.; Gutbrod, S. R.; Bonifas, A. P.; Su, Y.; Sulkin, M. S.; Lu, N.; Chung, H.-J.; Jang, K.-I.; Liu, Z.; Ying, M.; Lu, C.; Webb, R. C.; Kim, J.-S.; Laughner, J. I.; Cheng, H.; Liu, Y.; Ameen, A.; Jeong, J.-W.; Kim, G.-T.; Huang, Y.; Efimov, I. R.; Rogers, J. A. 3d Multifunctional Integumentary Membranes for Spatiotemporal Cardiac Measurements and Stimulation across the Entire Epicardium. *Nat. Commun.* **2014**, *5*, 3329.
(45) Yu, K. J.; Kuzum, D.; Hwang, S.-W.; Kim, B. H.; Juul, H.; Kim, N. H.; Won, S. M.; Chiang, K.; Trumpis, M.; Richardson, A. G.; Cheng, H.; Fang, H.; Thompson, M.; Bink, H.; Talos, D.; Seo, K. J.; Lee, H. N.; Kang, S.-K.; Kim, J.-H.; Lee, J. Y.; Huang, Y.; Jensen, F. E.; Dichter, M. A.; Lucas, T. H.; Viventi, J.; Litt, B.; Rogers, J. A. Bioresorbable Silicon Electronics for Transient Spatiotemporal Mapping of Electrical Activity from the Cerebral Cortex. *Nat. Mater.* **2016**, *15*, 782−791.
(46) Fang, H.; Yu, K. J.; Gloschat, C.; Yang, Z.; Song, E.; Chiang, C.-H.; Zhao, J.; Won, S. M.; Xu, S.; Trumpis, M.; Zhong, Y.; Han, S. W.; Xue, Y.; Xu, D.; Choi, S. W.; Cauwenberghs, G.; Kay, M.; Huang, Y.; Viventi, J.; Efimov, I. R.; Rogers, J. A. Capacitively Coupled Arrays of Multiplexed Flexible Silicon Transistors for Long-Term Cardiac Electrophysiology. *Nat. Biomed. Eng.* **2017**, *1*, 0038.
(47) Chang, J.-K.; Emon, M. B.; Li, C.-S.; Yang, Q.; Chang, H.-P.; Yang, Z.; Wu, C.-I.; Saif, M. T.; Rogers, J. A. Cytotoxicity and in Vitro Degradation Kinetics of Foundry-Compatible Semiconductor Nanomembranes and Electronic Microcomponents. *ACS Nano* **2018**, DOI: 10.1021/acsnano.8b04513.
(48) Kang, S.-K.; Hwang, S.-W.; Yu, S.; Seo, J.-H.; Corbin, E. A.; Shin, J.; Wie, D. S.; Bashir, R.; Ma, Z.; Rogers, J. A. Biodegradable Thin Metal Foils and Spin-On Glass Materials for Transient Electronics. *Adv. Funct. Mater.* **2015**, *25*, 1789−1797.
(49) Jin, S. H.; Kang, S.-K.; Cho, I.-T.; Han, S. Y.; Chung, H. U.; Lee, D. J.; Shin, J.; Baek, G. W.; Kim, T.-i.; Lee, J.-H.; Rogers, J. A. Water-Soluble Thin Film Transistors and Circuits Based on Amorphous Indium-Gallium-Zinc Oxide. *ACS Appl. Mater. Interfaces* **2015**, *7*, 8268−8274.
(50) Cerqueira, M. A.; Souza, B. W. S.; Simões, J.; Teixeira, J. A.; Domingues, M. R. M.; Coimbra, M. A.; Vicente, A. A. Structural and Thermal Characterization of Galactomannans from Non-Conventional Sources. *Carbohydr. Polym.* **2011**, *83*, 179−185.
(51) Pawar, H. A.; Lalitha, K. G. Isolation, Purification and Characterization of Galactomannans as an Excipient from Senna Tora Seeds. *Int. J. Biol. Macromol.* **2014**, *65*, 167−175.
(52) Pablyanalr, C.; Ícarogp, V.; Ângelamc, A.; de Paula, R. C. M.; Feitosa, J. P. A. Isolation and Characterization of Galactomannan from Dimorphandra Gardneriana Tul. Seeds as a Potential Guar Gum Substitute. *Food Hydrocolloids* **2009**, *23*, 880−885.
(53) Ganter, J. L. M. S.; Reicher, F. Water-Soluble Galactomannans from Seeds of Mimosaceae Spp. *Bioresour. Technol.* **1999**, *68*, 55−62.
(54) Muschin, T.; Yoshida, T. Structural Analysis of Galactomannans by Nmr Spectroscopy. *Carbohydr. Polym.* **2012**, *87*, 1893−1898.
(55) Bowen, P. K.; Drelich, J.; Goldman, J. Zinc Exhibits Ideal Physiological Corrosion Behavior for Bioabsorbable Stents. *Adv. Mater.* **2013**, *25*, 2577−2582.
(56) Trumbo, P.; Yates, A. A.; Schlicker, S.; Poos, M. Dietary Reference Intakes: Vitamin a, Vitamin K, Arsenic, Boron, Chromium, Copper, Iodine, Iron, Manganese, Molybdenum, Nickel, Silicon, Vanadium, and Zinc. *J. Am. Diet. Assoc.* **2001**, *101*, 294−301.
(57) Pietenpol, W. B.; Miley, H. A. Electrical Resistivities and Temperature Coefficients of Lead, Tin, Zinc and Bismuth in the Solid and Liquid States. *Phys. Rev.* **1929**, *34*, 1588−1600.
(58) Sondheimer, E. H. The Mean Free Path of Electrons in Metals. *Adv. Phys.* **1952**, *1*, 1−42.
(59) Webb, R. C.; Bonifas, A. P.; Behnaz, A.; Zhang, Y.; Yu, K. J.; Cheng, H.; Shi, M.; Bian, Z.; Liu, Z.; Kim, Y.-S.; Yeo, W.-H.; Park, J. S.; Song, J.; Li, Y.; Huang, Y.; Gorbach, A. M.; Rogers, J. A. Ultrathin Conformal Devices for Precise and Continuous Thermal Characterization of Human Skin. *Nat. Mater.* **2013**, *12*, 938−944.
(60) Sun, Y.; Choi, W. M.; Jiang, H.; Huang, Y. Y.; Rogers, J. A. Controlled Buckling of Semiconductor Nanoribbons for Stretchable Electronics. *Nat. Nanotechnol.* **2006**, *1*, 201−207.
(61) Wang, S.; Li, M.; Wu, J.; Kim, D.-H.; Lu, N.; Su, Y.; Kang, Z.; Huang, Y.; Rogers, J. A. Mechanics of Epidermal Electronics. *J. Appl. Mech.* **2012**, *79*, 031022.
(62) Pei, W.; Zhang, H.; Wang, Y.; Guo, X.; Xing, X.; Huang, Y.; Xie, Y.; Yang, X.; Chen, H. Skin-Potential Variation Insensitive Dry Electrodes for Ecg Recording. *IEEE Trans. Biomed. Eng.* **2017**, *64*, 463−470.
(63) Luo, Y.; Hargraves, R. H.; Belle, A.; Bai, O.; Qi, X.; Ward, K. R.; Pfaffenberger, M. P.; Najarian, K. A Hierarchical Method for Removal of Baseline Drift from Biomedical Signals: Application in Ecg Analysis. *Sci. World J.* **2013**, *2013*. DOI: 10.1155/2013/896056
(64) Gartler, J.; Robinson, B.; Burton, K.; Clucas, L. Carbonaceous Soil Amendments to Biofortify Crop Plants with Zinc. *Sci. Total Environ.* **2013**, *465*, 308−313.

DOI: 10.1021/acsami.8b11682
ACS Appl. Mater. Interfaces XXXX, XXX, XXX−XXX